R-03-19

Canister positioning

Influence of fracture system on deposition hole stability

Harald Hökmark, Clay Technology AB

November 2003

Svensk Kärnbränslehantering AB
Swedish Nuclear Fuel
and Waste Management Co
Box 5864
SE-102 40 Stockholm Sweden
Tel 08-459 84 00
+46 8 459 84 00
Fax 08-661 57 19
+46 8 661 57 19

ISSN 1402-3091
SKB Rapport R-03-19

Canister positioning

Influence of fracture system on deposition hole stability

Harald Hökmark, Clay Technology AB

November 2003

Keywords: canister position, nearfield rock, DFN model, stability, deposition hole, 3DEC, FracMan.

Abstract

The study concerns the mechanical behaviour of rock surrounding tunnels and deposition holes in a nuclear waste repository. The mechanical effects of tunnel excavation and deposition hole excavation are investigated by use of a tunnel scale numerical model representing a part of a KBS-3 type repository. The excavation geometry, the initial pre-mining state of stress, and the geometrical features of the fracture system are defined according to conditions that prevail in the TBM tunnel rock mass in Äspö HRL. Comparisons are made between results obtained without consideration of fractures and results obtained with inclusion of the fracture system. The focus is on the region around the intersection of a tunnel and a deposition hole. A general conclusion is that a fracture system of the type found in the TBM rock mass does not have a decisive influence on the stability of the deposition holes. To estimate the expected extent of spalling, information about other conditions, e.g. the orientation of the initial stresses and the strength properties of the intact rock, is more important than detailed information about the fracture system.

Sammanfattning

Studien avser det mekaniska uppförandet hos berget kring tunnlar och deponeringshål i ett slutförvar för använt kärnbränsle. De mekaniska effekterna av tunnel- och deponeringshålsuttag undersöks i en numerisk model i tunnelskala av en del av ett KBS-3-förvar. Hålrumsgeometrin, det ostörda primära bergspänningstillståndet och de geometriska egenskaperna hos spricksystemet definieras i enlighet med de förhållanden som råder i bergmassan kring TBM-tunneln i Äspö HRL. Jämförelser görs mellan resultat som erhållits utan att beakta sprickorna och resultat som erhållits genom att inkludera några olika varianter av spricksystemet. Undersökningen fokuserar på området kring skärningen mellan tunnelgolv och deponeringshål. En allmän slutsats är att spricksystem av den typ som finns kring TBM tunneln inte har något avgörande inflytande på deponeringshålens stabilitet. För att bedöma förväntad omfattning av smällberg är kunskap om andra förhållande, t ex spänningarnas orientering och hållfastheten hos det intakta berget, viktigare än detaljerad kunskap om spricksystemet.

Contents

1 Introduction and background

The fraction of possible emplacement hole positions along a KBS-3 type nuclear waste deposition tunnel that can actually be used for deposition of waste canisters will be an important issue during different stages of decision-making within the repository site selection, design and construction phases. Some criteria for rejecting positions will deal with long-time performance aspects, e.g. expected post-closure groundwater flow in fractures that intersect the deposition hole and connect to the tunnel or to nearby major fracture zones. Other criteria will have to do with construction aspects, e.g. inflow into the open deposition hole during construction and emplacement, or the mechanical stability of the deposition hole walls.

Acceptance or rejection of individual deposition hole positions will depend on the expected consequences of a number of processes: excavation of tunnel and emplacement hole, interaction with the swelling bentonite buffer, heating and subsequent cooling. Additional, hypothetical, processes include effects of glaciation and seismic events. The consequences of these processes may depend on the arrangement of fractures in the nearfield, on the mechanical properties of the nearfield- and farfield rock, and on the initial stress field.

Only mechanical aspects of the acceptance/rejection procedure are being addressed in this numerical study. The TBM tunnel in the Äspö HRL has been selected to represent a deposition tunnel in the central part of a hypothetical KBS-3 type repository. The fracture system is based on a statistical representation of trace data obtained from the walls of the TBM tunnel. The numerical tool being used for the study is the three-dimensional distinct element code 3DEC, which is a well established code, developed specifically for analysing the behaviour of rock containing multiple, intersecting fractures /1-1/. Only effects of tunnel- and deposition hole excavation are analysed, i.e. not effects of the thermal load or effects of buffer/rock interactions.

In a previous 3DEC study, also the effects of the thermal pulse and of the pressure exerted on the deposition hole walls by the swelling buffer were analysed /1-2/. In that study, however, the rock mass surrounding the TBM tunnel was modelled as an elastic continuum, i.e. no fractures were included. The main conclusion of the previous study was that, as far as secondary stresses and risks of failure in the nearfield rock are concerned, the most important factor is the orientation of the initial stresses relative to the orientation of the tunnel axis. It was also found that, for the stress field assumed to prevail in the TBM tunnel rock mass, the excavation-induced stress redistribution was more important than effects of the thermal load. The effects of the swelling pressure were minor.

Figure 1-1 shows the geometry of the continuum model. The tunnel diameter is 5 m, and the deposition hole diameter is 1.6 m. This model was slightly modified and then used as point of departure for the fractured rock mass model analysed in this report.

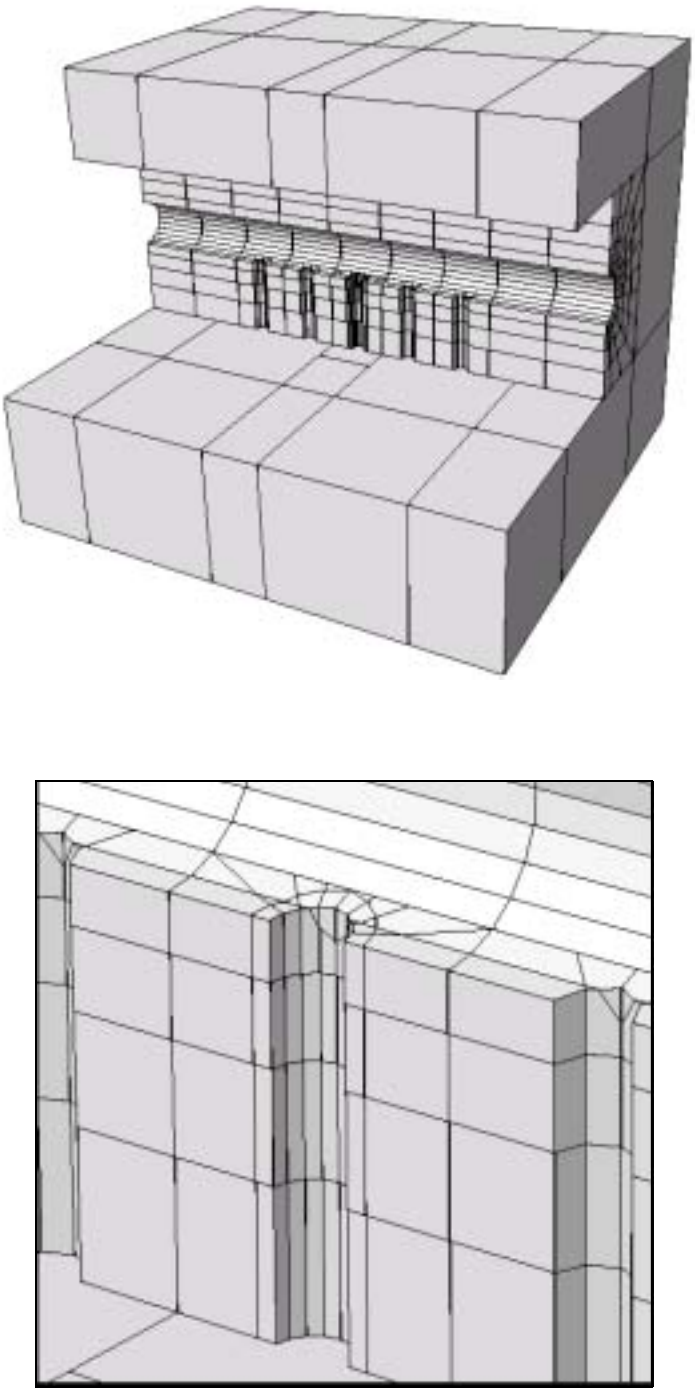

Figure 1-1. *Geometry of the continuum model. Upper: Full model with outer blocks hidden to display the interior. Lower: Close-up view of the central deposition hole.*

2 Objectives

The objective of this study is to find out how the mechanical response to excavation of tunnel and deposition hole is influenced by the presence of a fracture system that conforms in a statistical sense with the fracture system in the rock mass surrounding the TBM tunnel in Äspö HRL.

3 Model description

3.1 General

The 3DEC model regards a box-shaped portion of the rock mass around the TBM tunnel in Äspö HRL. The fractures, the initial stresses and the rock mass properties are defined accordingly.

3.2 Model dimensions and excavation geometry

Figure 3-1, left part, shows the outlines of the model. The TBM tunnel and three deposition holes with a diameter of 1.6 m are included. The x-axis coincides with the tunnel axis. The origin is in the intersection between tunnel axis and the axis of the central deposition hole. The y-axis is vertical, and the z-axis is horizontal and perpendicular to the tunnel axis. The length (x) of the model is 42 m. The height (y) is 45 m and the width (z) is 50 m. The regular orthogonal and radial cuts are construction planes, not fractures. Real fractures were modelled in an inner 28 m × 30 m × 30 m volume (Figure 3-1, right part)

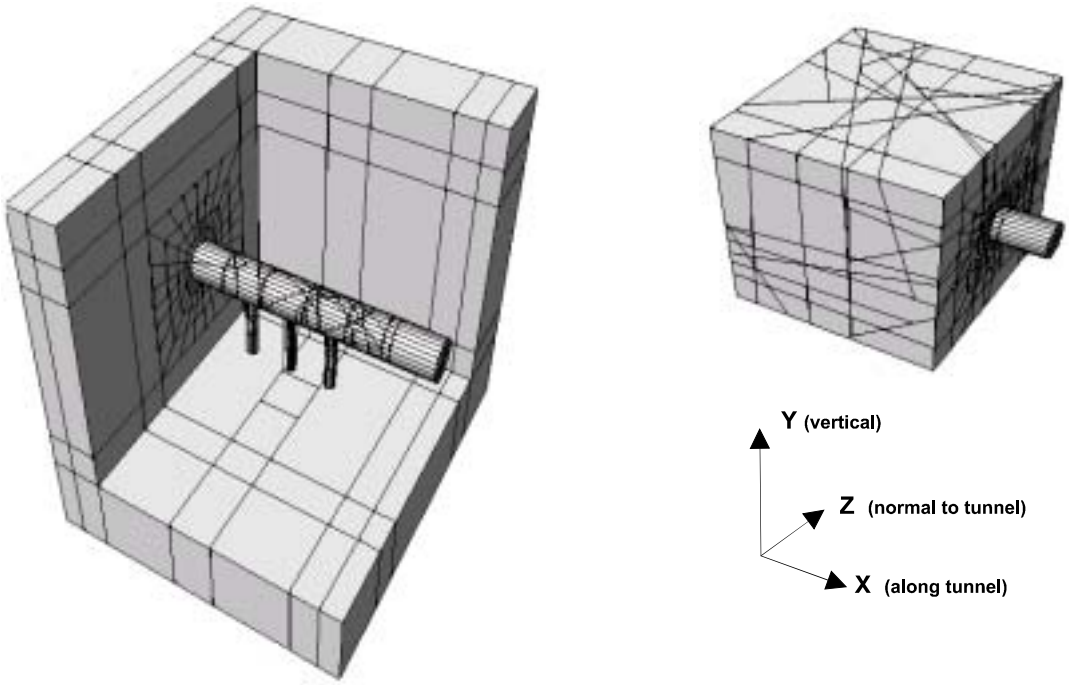

Figure 3-1. *3DEC model with tunnel and three deposition holes. The right part shows inner box, in which fractures were modelled. The lower right part shows orientation of the co-ordinate axes.*

3.3 Fracture geometry

3.3.1 General

The fracture geometry was defined by use of the Discrete Fracture Network model assumed to apply for the TBM region in the Äspö HRL. The DFN model, which is based on geometrical data for 470 fractures mapped in the TBM tunnel (Follin and Hermansson, 1997 /3-1/), describes the fracture system statistically. Follin and Hermansson generated 30 realisations of the statistical DFN model by use of the FracMan code. According to the DFN model, the fracture intensity is 0.47 m^2 of fracture area per cubic metre of rock mass.

3.3.2 FracMan realisations

The FracMan realisations of the TBM tunnel rock mass DFN model regard cubes of 20 m side-length. In the DFN model realisation, fractures have a radius, a location and an orientation. Fractures are either completely contained within the cube or intersect sides of the cube. The FracMan realisations approximate the geometry of individual fractures with planar hexagons. Each hexagon is represented by a list of node co-ordinates and by the fracture plane unit normal. The nodes are hexagon corners, points of intersection between cube sides and fracture edges, or points on intersections between cube edges and the fracture plane (Figure 3-2).

Out of the 30 FracMan realisations of the DFN model generated by Follin and Hermansson, realisation #1 was picked arbitrarily for the 3DEC analysis. This particular realisation includes 46 fractures with radii ranging between 2 m and about 15 m. The fracture intensity is 0.48 m^2/m^3.

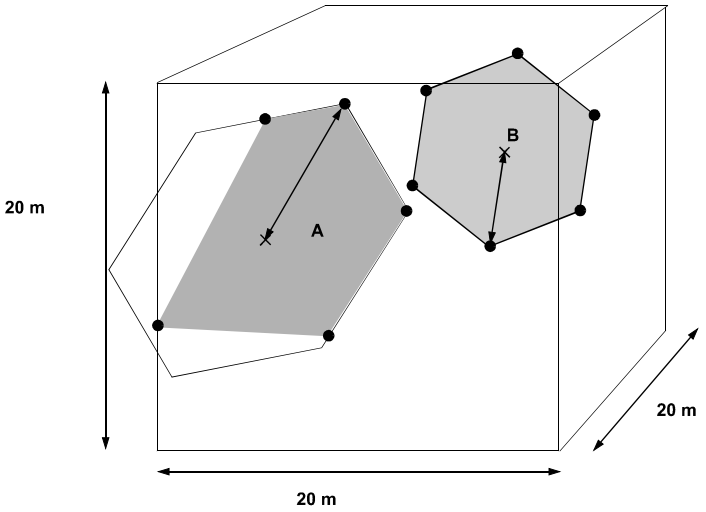

Figure 3-2. *FracMan representation of fracture that intersects sides of the cube being modelled (A) and fracture fully contained within the cube (B).*

3.3.3 Conversion to 3DEC input

The FracMan realisations of the DFN model of the TBM tunnel rock mass are based on the ÄSPÖ HRL co-ordinate system. In this system, the tunnel is not aligned with any of the co-ordinate axes. In 3DEC models containing regularly shaped excavations, it is expedient to define axes that account for the symmetry of the problem, cf section 3.2. Therefore, the FracMan fracture data, i.e. node co-ordinates and unit normals, were transformed to 3DEC co-ordinates. In 3DEC, fracture orientations are given by the dip angle (DIP) and the dip direction angle (DD), rather than by the unit normal. Table 3-1 shows the FracMan fracture data converted for use as 3DEC input.

For fractures #7, #14, #23, #31 and #42, only one hexagon corner was contained within the FracMan cube. The radii and the centre co-ordinates of such one-corner fractures cannot be calculated from the list of nodes. If the fracture does not extend deep into the cube, then these parameters cannot even be estimated. On the other hand, in that case the fracture cannot interact with the central parts of the model, which means that it does not have to be considered. This applies for fractures #14, #23, #31 and #42. For fracture #7, the radius was approximated to be 16 m and the centre to be in the origin (i.e. at the intersection of the tunnel axis with the axis of the central deposition hole). Figure 3-3 shows a plot representation of the 46 fracture planes.

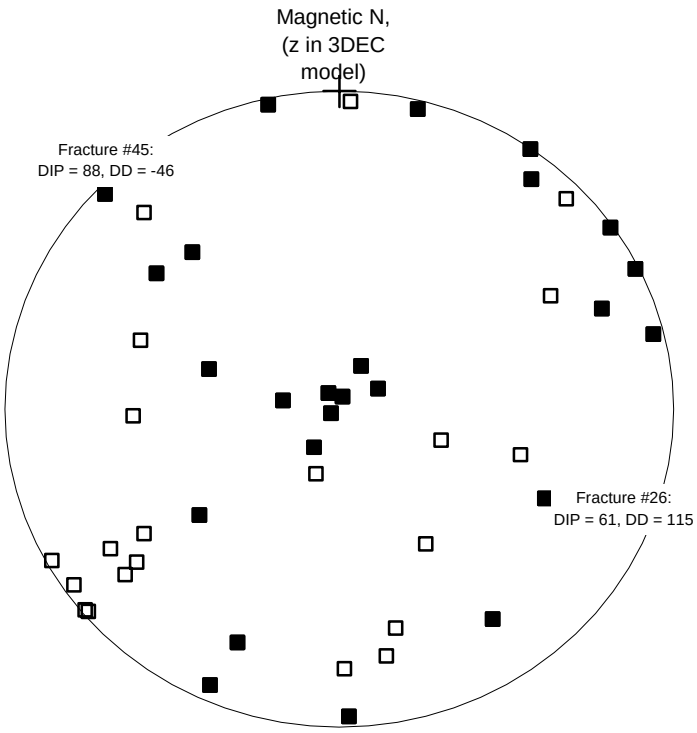

***Figure 3-3**. Plot representation of all 46 fracture planes. Filled symbols represent fractures actually included in the 3DEC model (see below). DIP angles are zero in the centre and 90 degrees at the plot periphery, while DIP Directions are given clockwise with respect to the positive z-axis. (Fractures #26 and #45 are labelled to illustrate sense of DIP and DD.)*

Table 3-1. 3DEC input for realisation #1 fractures.

Realisation #1				Fracture centre co-ordinates		
Fracture #	**DIP**	**DD***	**Radius**	**x**	**y**	**z**
01	2.51	–118.54	5.18	–4.98	–7.45	–2.01
02	73,18	–122,76	6,48	3,86	–4,62	6,51
03	87,03	–124,88	3,60	0,38	2,93	4,17
04	76,47	–43,38	6,43	–6,14	–8,78	8,52
05	44,73	148,58	6,72	–1,84	–9,38	8,30
06	89,07	63,56	10,26	–3,16	–12,02	–2,58
07	15,31	–80,82				
08	19,38	–161,26	4,63	–5,85	–9,86	6,85
09	63,83	166,24	7,04	–5,49	–9,37	2,85
10	12,78	–148,22	8,52	–1,21	1,29	–9,75
11	85,52	–156,02	5,04	–0,45	2,46	0,32
12	88,55	–130,35	3,78	5,61	2,96	–5,42
13	11,98	61,09	6,73	5,42	3,18	8,04
14	69,66	–128,46				
15	89,26	54,91	5,21	–8,03	–4,50	–0,49
16	88,21	–12,47	7,20	7,16	4,44	6,06
17	87,17	75,96	5,26	–6,90	2,20	3,71
18	72,43	145,19	10,70	–1,38	–7,54	–8,86
19	76,21	68,12	8,20	–0,01	5,65	7,73
20	62,37	–52,00	6,25	0,62	0,26	8,65
21	5,40	–32,55	14,86	8,68	–4,35	5,34
22	28,83	107,74	3,86	0,61	7,16	5,48
23	65,30	60,58				
24	87,10	2,03	4,58	–3,70	4,43	–8,12
25	83,07	38,50	5,62	7,57	3,22	0,80
26	60,90	114,56	5,20	0,73	–0,61	3,87
27	71,09	169,70	7,39	–8,25	–10,19	4,61
28	3,66	13,71	3,93	–4,50	–2,86	3,46
29	55,49	–91,98	6,42	9,75	–5,47	–7,35
30	73,55	178,92	5,57	10,80	–8,07	–6,13
31	88,96	230,24				
32	48,13	–128,65	6,46	3,30	–3,12	0,70
33	13,60	25,88	6,12	5,16	5,28	1,46
34	50,53	104,84	2,14	1,17	–4,09	–5,54
35	59,43	–41,65	6,72	–3,40	–4,12	–0,79
36	89,73	34,99	8,84	10,29	–5,48	–2,48
37	87,47	13,97	8,92	7,73	–3,13	–0,75
38	36,80	–72,15	7,52	4,73	–2,35	0,95
39	88,44	240,96	6,36	9,89	0,82	–5,23
40	63,28	–123,88	5,17	–9,69	–9,55	–2,26
41	56,88	–70,02	1,98	–9,43	–3,44	2,48
42	85,34	45,78				
43	71,51	–157,53	5,24	9,23	–3,65	–1,54
44	74,23	–129,16	4,12	6,56	–11,02	–6,22
45	87,60	–45,99	10,74	8,93	–7,76	5,06
46	87,07	178,29	8,77	–1,85	–12,35	8,60

*) Dip Directions (DD) are measured clockwise from the positive z-axis.

3.3.4 Fractures in the 3DEC model

3.3.4.1 Fracture cut planes

In the 3DEC code, cut planes split one ore many blocks into smaller blocks and are either just construction planes or actual fracture planes. Due to computer memory restrictions and run time considerations, the number of cut planes that can actually be accommodated in a 3DEC model is limited. Construction planes are usually regularly arranged, while fracture planes may be irregularly located and oriented. If the intended accuracy of the stress analysis requires a fine zoning, and the geometry is complicated with multiple intersecting excavations (which requires numerous construction cut planes as in the case here where deposition holes intersect a tunnel), then 46 intersecting and arbitrarily oriented fracture planes cannot be included. Therefore, only 25 out of the 46 DFN model fractures were included in the 3DEC model. Small fractures located far from the region of interest were ignored. The remaining 25 fractures were divided in two groups:

1. Fractures that interact directly with the region of interest, i.e. the region around the intersection between the tunnel and the central deposition hole.

2. Fractures at some distance from the region of interest.

Analyses were run with both groups of fractures (full set of fractures) and with omission of group 2 (reduced set of fractures).

Figure 3-4 shows the fracture cut planes. For visibility, the 25 cut planes are shown in four different plots. The two upper plots show group 1 fractures with labels denoting the FracMan fracture identities (Table 3-1). The two lower plots show group 2 fractures, but without fracture identity numbers.

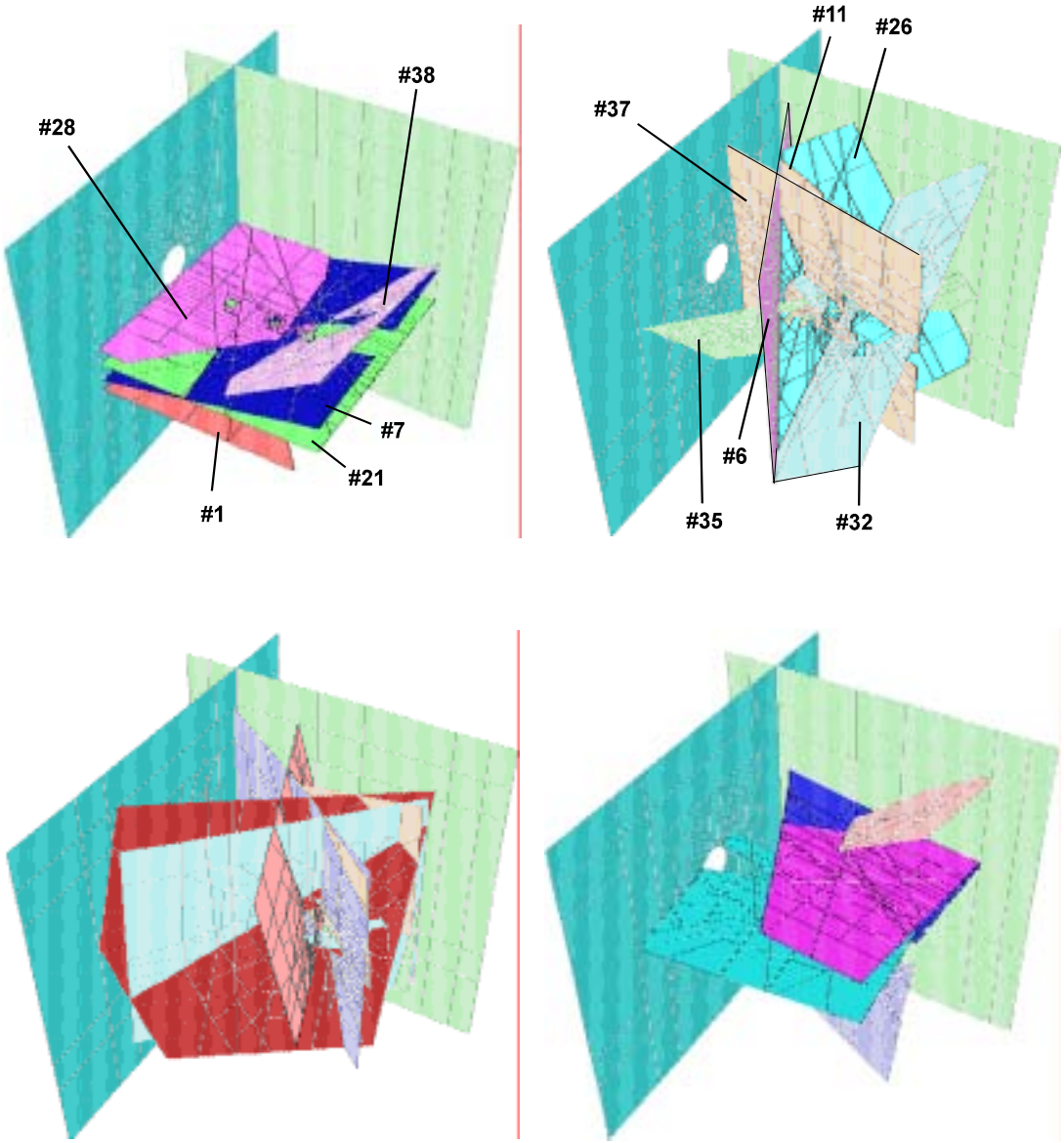

Figure 3-4. *Fracture cut planes. The upper plots show the reduced set. The full set includes also the fractures in the lower plots.*

3.3.4.2 Fractures

In 3DEC models, cut planes must terminate at intersections with other cut planes or at the model boundaries. This means that the rock mass is subdivided into blocks separated by cut planes. Systems of fractures such as in the DFN model realisations, where fractures may have unconnected edges or even may be completely disconnected from other fractures (cf Figure 3-2), cannot be modelled correctly in a geometrical sense. However, the mechanical equivalent of such a system can be obtained by assigning different mechanical properties to different parts of cut planes. This option is not available in the standard 1.5 version of 3DEC, but was added by Itasca Inc for the particular purpose of this study. A circular portion of a cut plane, corresponding to the geometry and size of the DFN fracture, can be given actual fracture properties, such as realistic values of friction and cohesion, while other parts are given fictive properties that inhibit relative block movements. Figure 3-5 shows the 3DEC representation of one particular fracture.

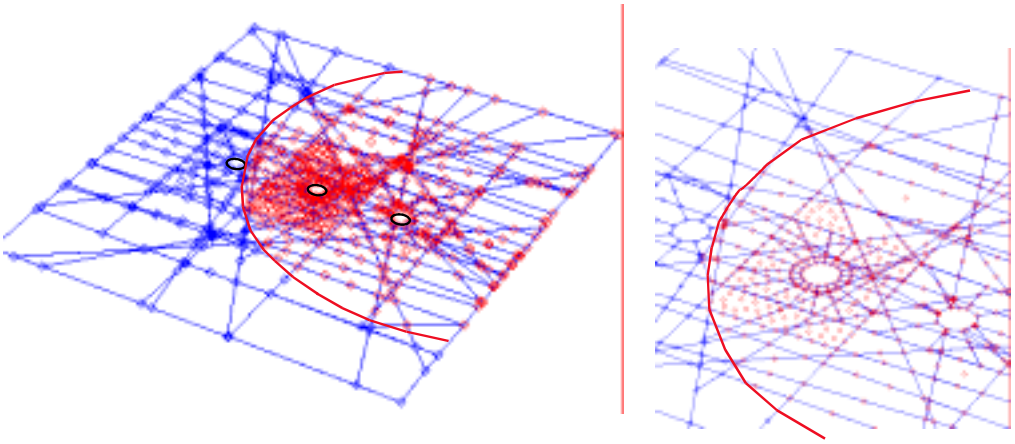

Figure 3-5. *Cut plane with circular fracture. This particular fracture (#21) dips 5.4 degrees and intersects two of the deposition holes. The radius is 14.9 m and the fracture centre is about 2 m below the tunnel floor.*

3.4 Material properties

3.4.1 Intact rock properties

The intact rock, i.e. the continuum material between fractures, was assumed to be isotropic, homogeneous and linearly elastic. The density was set to 2600 kg/m^3, Young's modulus to 40 GPa and Poisson's ratio to 0.2. This numbers are consistent with RMR values reported for the TBM tunnel /3-2/, and with rule-of-thumb expressions used for translating RMR values to material property values /3-3/.

3.4.2 Fracture properties

An ideally elastoplastic model with a Morh-Coulomb failure criterion was used for the fractures. This model does not account for nuances of the mechanical behaviour of fractures, e.g. stress dependent stiffnesses or changes in shear strength caused by damage done to asperities during shear, but the essence is well captured. In this study, the influence of the fracture system as a whole is analysed, not the detailed response of individual fractures. The elastoplastic model implies constant normal stiffness k_n and constant shear stiffness k_s. Here, k_n was set to 10 000 GPa/m and k_s to 20 GPa/m. These values are representative of single fractures in granitic rock /3-4/. The tensile strength was set to zero. The Mohr-Coulomb criterion gives the shear strength τ as

$$\tau = \tan \phi \cdot \sigma_n + c,$$

where ϕ is the friction angle, σ_n is the normal stress and c is the cohesion. The cohesion was set to zero, which is conservative. The friction angle was set to 40, 30 and 20 degrees. Laboratory tests on rock joint samples from Stripa have given residual friction angles of about 25 degrees /3-5/, laboratory test on rock joint samples from Äspö HRL have given residual friction angles of about 40 degrees /3-6/. In the first stages of shear movements, the apparent friction is often increased because of cohesion. For the Äspö HRL rock joint samples the corresponding peak friction angle amounted to between 45 and 60 degrees /3-6/. In addition, dilatancy usually contributes to the shear strength and increases the effective residual friction angle. In the material model used here, no peak shear strength and no dilatancy were assumed. Therefore, altogether, the shear strength is probably realistic/underestimated for the case of 30 degrees friction angle and realistic/overestimated for the case of 40 degrees. The case of 20 degrees friction angle is almost certainly conservative.

3.5 Initial stresses

The initial stress field was set according to measurements in borehole KA3068A /3-7/. That borehole is located at some distance from the TBM tunnel, and therefore the measurements are not fully accurate for the local TBM rock mass. The results are, however, reasonably representative with respect to stress level and stress anisotropy. The initial stresses are shown in Table 3-2. Bearings are given with respect to magnetic north.

Table 3-2. Initial Stresses.

Principal Stress	Magnitude [MPa]	Bearing [degr]	Dip [degr]
σ_1	28.9	287	13
σ_2	15.2	193	10
σ_3	08.5	067	73

3DEC Component	Normal stress			Shear stress		
	σ_{xx}	σ_{yy}	σ_{zz}	σ_{xy}	σ_{xz}	σ_{yz}
Magnitude [MPa]	–26.66	–9.79	–16.15	–4.66	3.72	0.14

3.6 Boundary conditions

All boundaries were fixed in all directions. This gives a slight underestimate of the mechanical response to excavation. The boundaries were however located sufficiently far away from the excavated rooms for boundary effects to be negligible.

3.7 Calculation sequence

The simulation sequence is outlined schematically below:

- Create outline of model with construction cut planes for definition of the excavation geometry and for defining regions of differently refined zoning.
- Define 25 cut planes to model the fractures, perform zoning of the continuum between the cut planes. Give all cut planes fictive fracture properties that inhibit relative block movements.
- Remove material in tunnel interior and calculate stresses and displacements in new elastic equilibrium state. Save state as M1.
- Remove material in deposition hole interior and calculate stresses and displacements in new equilibrium state. Save state as M2 (elastic model).
- Assign real fracture properties to circular portions of all 25 fracture cut planes according to the fracture geometry data. Set friction angle to 40 degrees, and calculate stresses and displacements in new equilibrium state. Save state as M3a. Then reduce the friction angle to 30 and 20 degrees with equilibrium calculations in between. Save states as M3b and M3c, respectively (“full set of fractures”).
- Restart state M2 and proceed as above, but assign real fracture properties only to the selected subset. Save states M4a, M4b and M4c (“reduced set of fractures”).

The displacements in models M2, M3 (a, b, c) and M4 (a, b, c) represent the combined effects of tunnel and deposition hole excavation. To separate these effects additional simulations were performed as follows:

- Restart state M1, and assign fracture properties to full set of fractures. Set friction angle to 40 degrees and calculate stresses and displacements in new equilibrium state. Save state as M5a, then obtain and save states M5b and M5c with friction angles 30 and 20 degrees, respectively.

- Then, using M5c as point of departure, reset all displacements to zero (accumulated displacements are stored in the 3DEC data arrays but not used in the 3DEC equations, which means that they can be reset without affecting the stress analysis) and remove material in the interior of the deposition holes. Calculate stresses and displacements in new equilibrium state and save as state M6.

For the lowest friction angle, 20 degrees, the rock mass is not in equilibrium under the applied stresses. Some fractures would undergo slip even without the stress redistribution caused by the excavations. However, no initial equilibrium calculations were performed in order to allow for initial displacements and associated modification of the initial stress field to take place prior to performing the excavation calculations. This means that the effects of excavation are overestimated for the case of 20 degrees friction angle, also if the friction angle in fact should be that small.

4 Results

4.1 General

In 3DEC, the intact rock blocks, i.e. the continuum material between cut planes, are subdivided into tetrahedral zones in order to allow for block deformability. The degree of refinement is set by the user with respect to the required accuracy of the internal stress/deformation analysis. In this study, the zoning is dense around the intersection between the central deposition hole and the tunnel and gradually coarser at larger distances from that region.

Forces are transferred from block to block across cut planes by means of contacts that are distributed over the cut plane and along block edges. If the zoning of the blocks is fine, there will a dense contact distribution.

Rock displacements are evaluated in the corners of the tetrahedral zones, relative block motions (i.e. fracture displacements) in the contacts and stresses in the zone centroids. In vector or tensor plots, absolute magnitudes are colour-coded, while the lengths of the symbols scale to the projection onto the viewing plane.

4.2 Rock displacements

Figure 4-1 shows rock displacements in a horizontal section through an annular region around the central deposition hole. The horizontal section is at a depth of 5 cm below the tunnel floor. The displacements shown in this plot represent the combined effects of tunnel excavation and deposition hole excavation. Three assumptions regarding the fracture system are considered: No fractures, full set of fractures and reduced set of fractures. The following observations can be made:

- The major part of the deformations is due to elastic rock mass response. In the most conservative case (full set, 20 degrees friction angle), fracture deformations contributed at most 30%.

- Inclusion of all 25 fractures (full set) gave insignificant increase of deformations compared to including only fractures located close to the region around the upper part of the central borehole (reduced set).

Figure 4-2 shows corresponding results at 3 m depth below the tunnel floor. The same general observations as for the section just below the tunnel floor apply, i.e. deformations are mainly elastic and fractures at some distance from the hole, i.e. those not included in the reduced set, have a very modest influence.

Figure 4-3 shows rock displacement in two horizontal sections: 5 cm below the tunnel floor and 3 m below the tunnel floor. The figure regards the case giving the largest deformations (full set, 20 degr friction angle). Here the effects of tunnel excavation and deposition hole excavation are separated. The following observation can be made:

- The effects of tunnel excavation are small but, relatively seen, considerably larger than the effects of deposition hole excavation. This applies also for points on the walls of the deposition hole at 3 m depth.

Figure 4-4 shows rock displacements in a vertical section through the central deposition hole. In the upper part the combined effects of tunnel excavation and deposition hole excavation are compared for two cases: the elastic case (no fractures) and the case giving the largest deformations (full set, friction angle 20 degr). The following observation can be made:

- The major part of the deformations is due to the elastic response. Fracture deformations contributed at most 30%, i.e. for the most conservative case.

In the lower part of Figure 4-4, effects of tunnel excavation and deposition hole excavation are separated. The following observation can be made:

- Even at the boundary of the deposition hole, the effects of tunnel excavation are, relatively seen, considerably larger than the effects of deposition hole excavation.

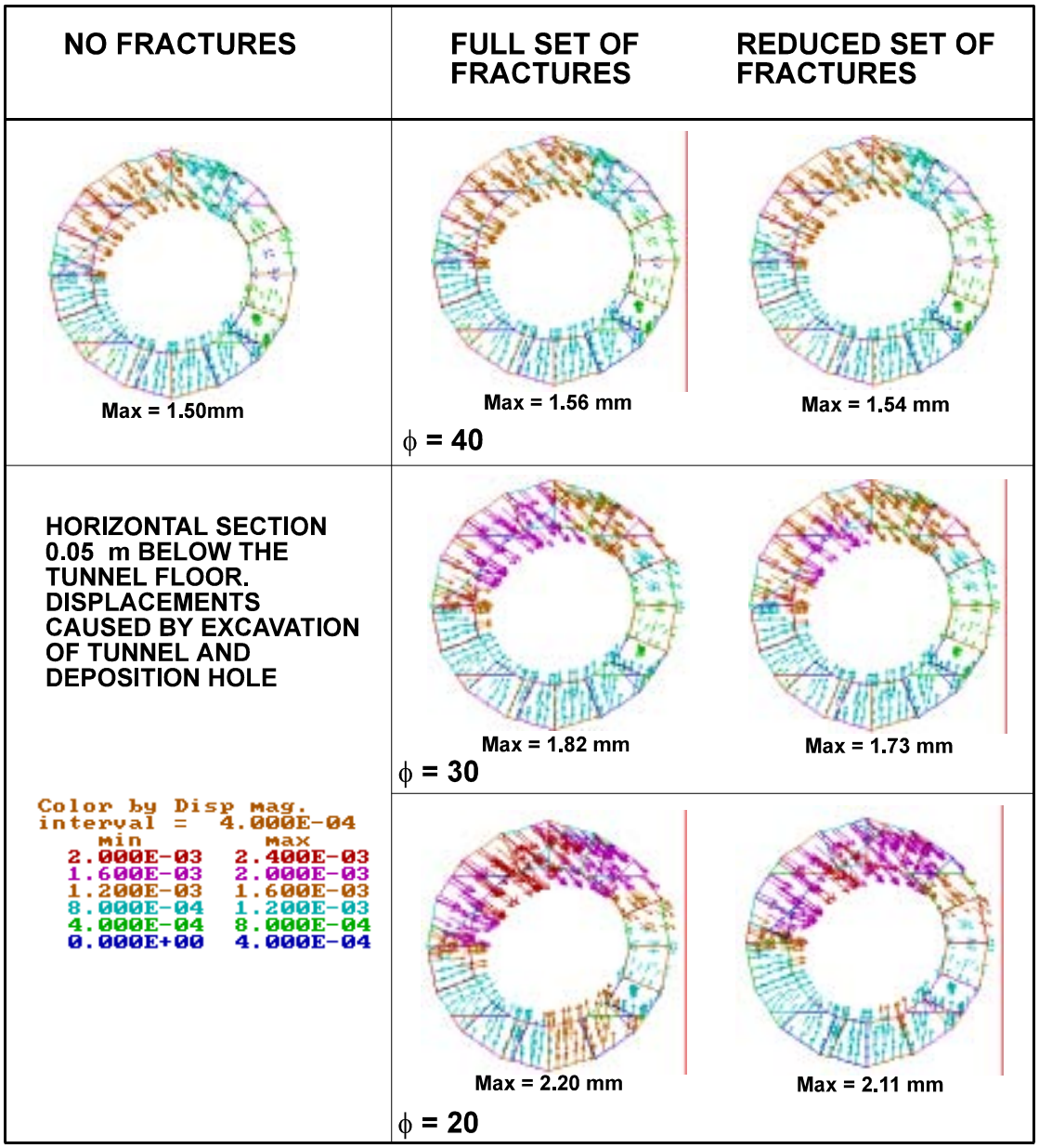

Figure 4-1. *Displacement of gridpoints in annular region around the central deposition hole. Displacements are accumulated effects of tunnel and deposition hole excavation. The colour code regards the total magnitude, while the vector symbol lengths are projections onto the viewing plane.*

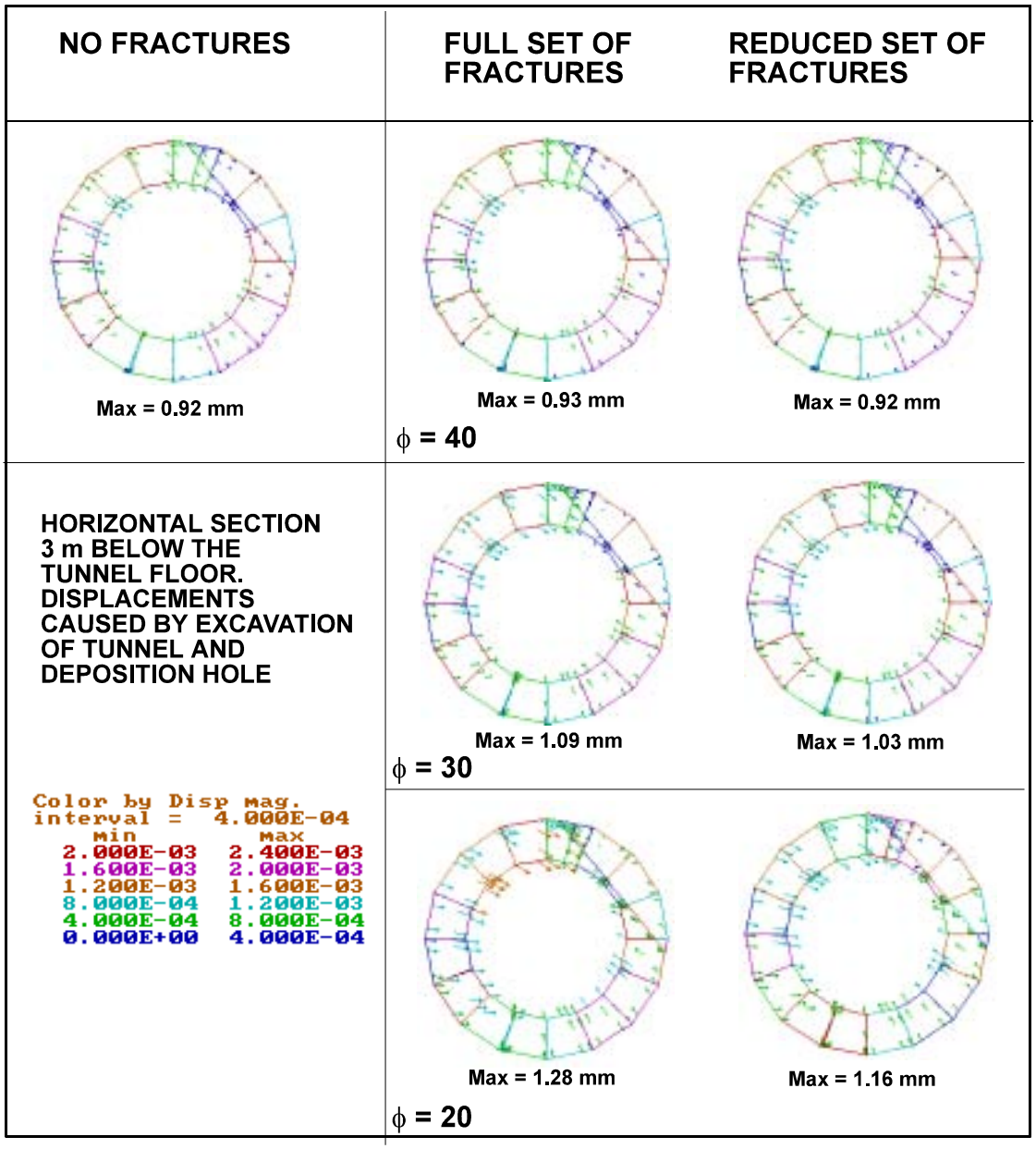

Figure 4-2. *Displacement of gridpoints in annular region around the central deposition hole. Displacements are accumulated effects of tunnel and deposition hole excavation. The colour code regards the total magnitude, while the vector symbol lengths are projections onto the viewing plane.*

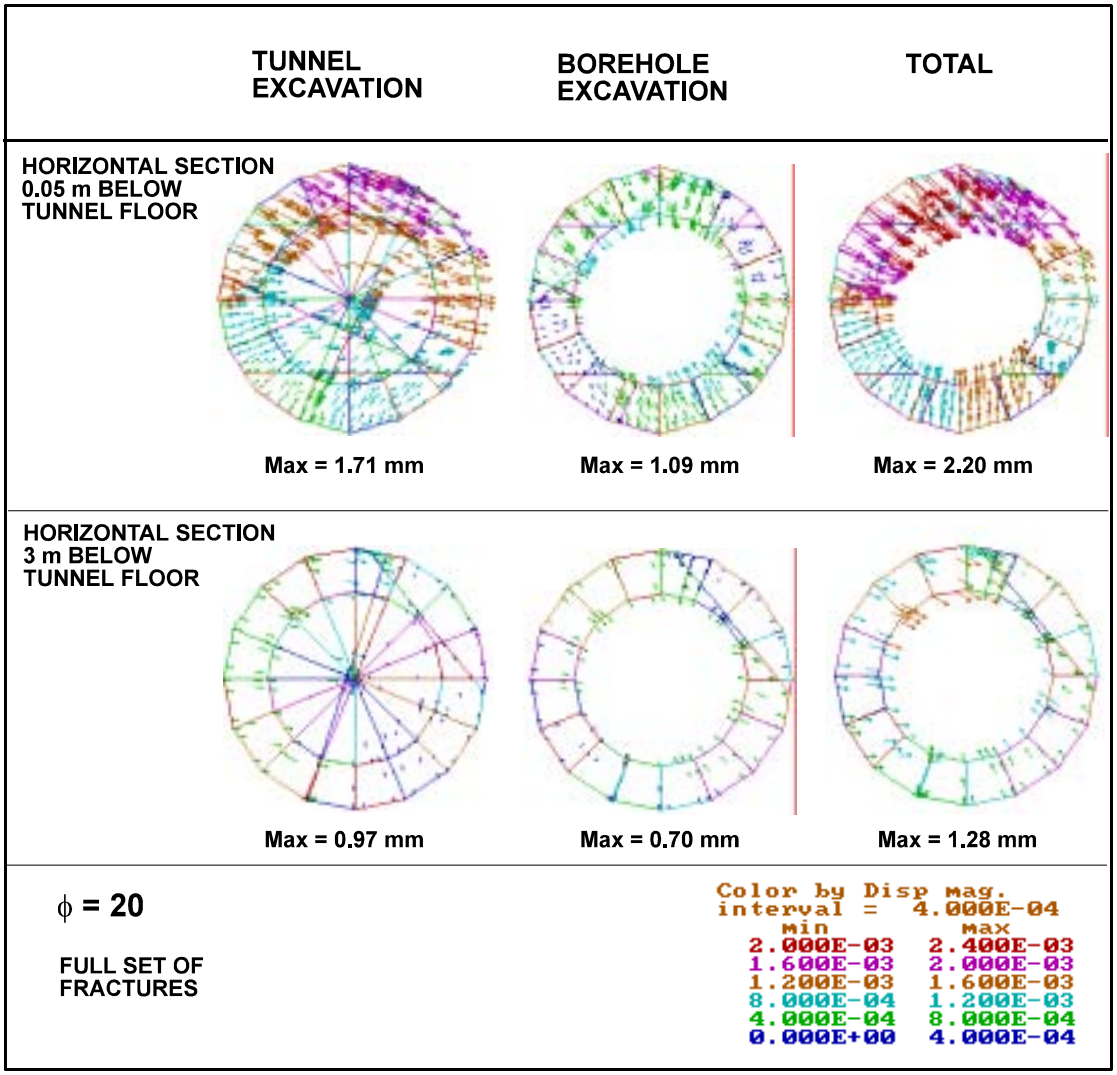

Figure 4-3. *Displacement of gridpoints in annular region around the central deposition hole. Displacements caused by tunnel excavation (left) and deposition hole excavation (middle) give total accumulated displacement (right). The colour code regards the total magnitude, while the vector symbol lengths are projections onto the viewing plane.*

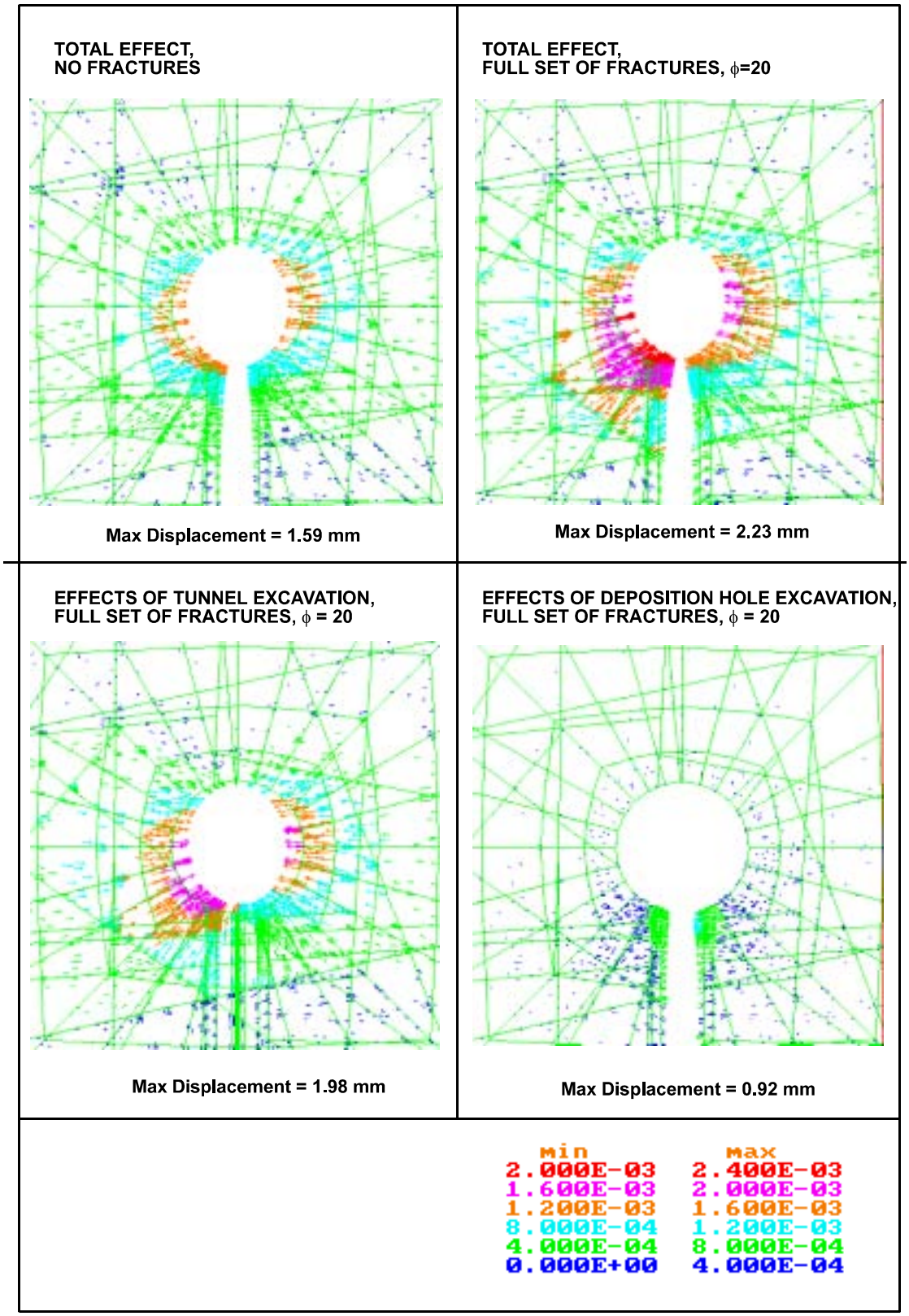

Figure 4-4. *Rock displacements in vertical section through the model centre.*

4.3 Fracture shear displacements

Figure 4-5 shows fracture shear displacements caused by tunnel excavation and deposition hole excavation. The upper part shows the result when all 25 fractures are included (full set). The lower part shows the result when only the most significant fractures, i.e. those that intersect the central parts of the model, are included (reduced set). The left parts show a transversal vertical section through the central deposition hole. The right parts show a longitudinal vertical section through the tunnel axis. Contours of the deposition holes are indicated with dotted lines. In the upper part, the most significant fractures are labelled with their fracture identity number according to Table 3-1 (cf Figure 3-4). The colour code gives absolute displacements, while the lengths of the vectors scale to projections onto the viewing plane. The following observations can be made:

- The omission of less significant fractures (those not included in the full set) did not have any important influence on the results in the central parts of the model. Displacement magnitudes were reduced by about 10%. This applies for both sections.

- The most significant shear displacements occur on fractures that intersect the tunnel in oblique angles. The max displacements are found on the tunnel/fracture intersections.

In Figure 4-6, the effects of tunnel and deposition hole excavation are separated. Note that the combined effects are obtained by addition of vectors, not of absolute values. Therefore, the absolute values found in the tunnel excavation stage and the deposition hole excavation stage do not add up to the values found in Figure 4-5. The following observation can be made:

- Even at the walls of the deposition hole, the tunnel excavation gave larger effects than the excavation of the deposition hole itself.

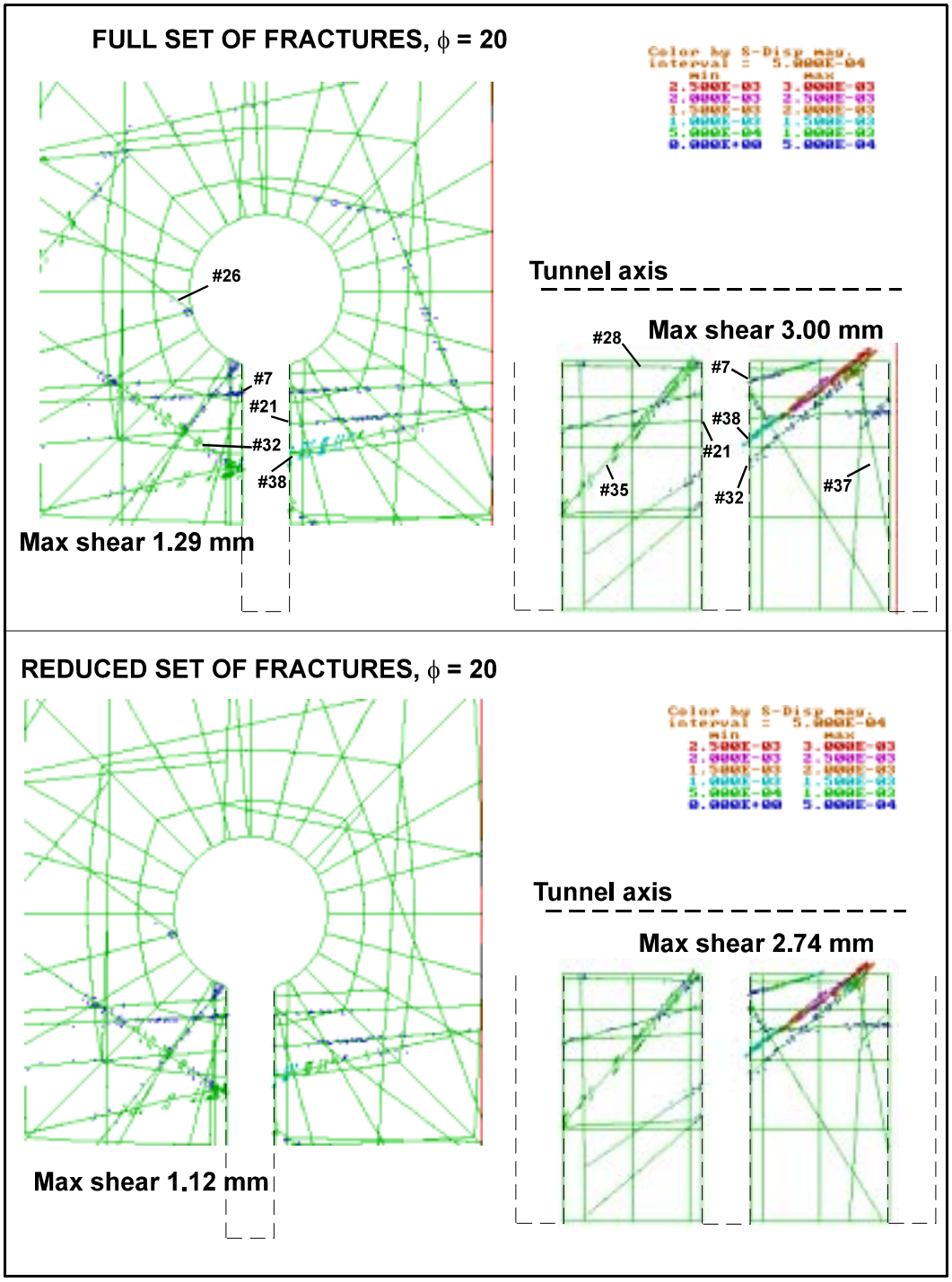

Figure 4-5. *Fracture shear displacements in vertical sections trough the model centre. The displacements are the accumulated effects of tunnel- and deposition hole excavations.*

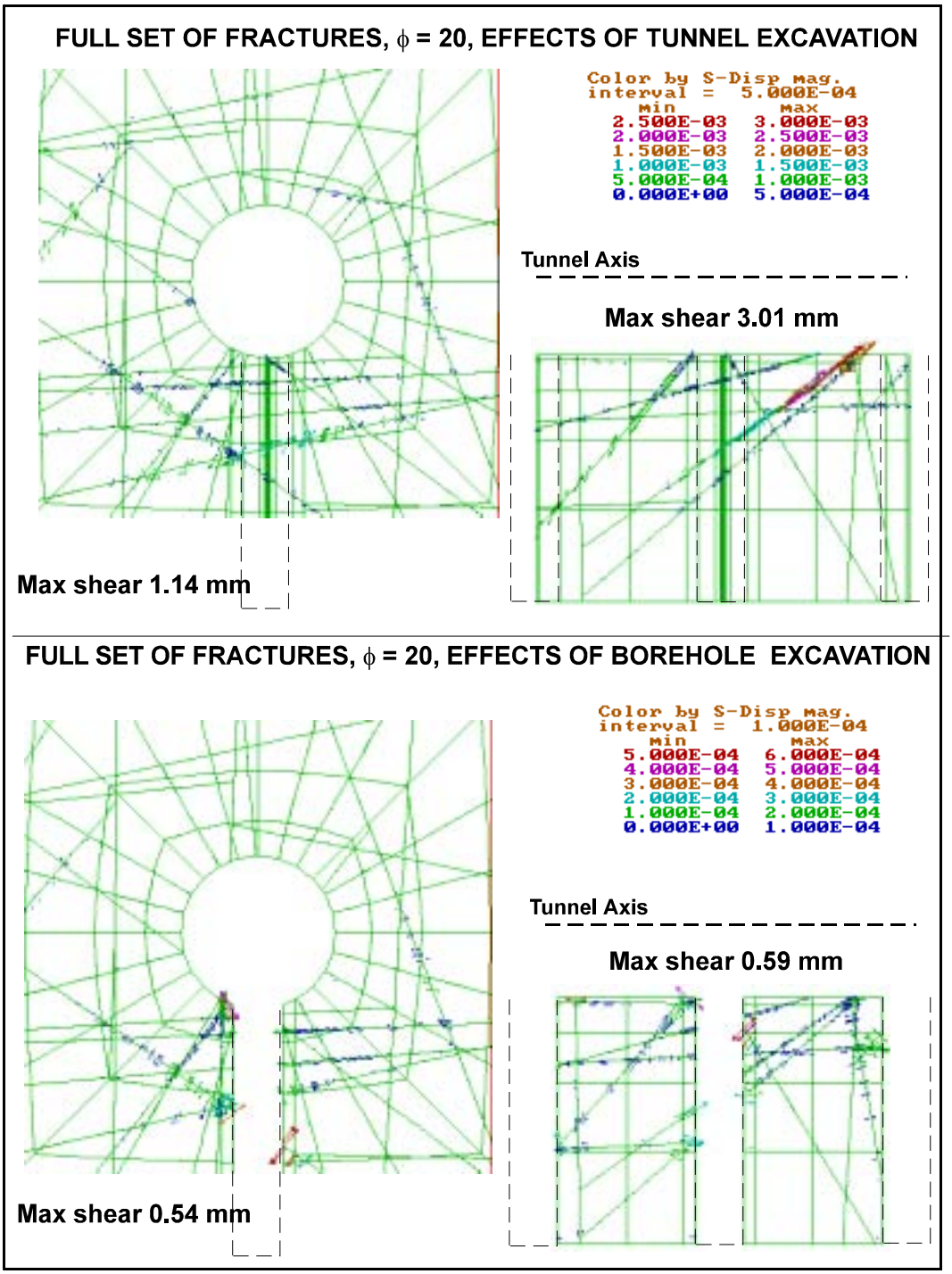

Figure 4-6. *Fracture shear displacements in vertical sections trough the model centre. The displacements are effects of tunnel excavation (upper) and deposition hole excavation (lower).*

4.3 Stresses

Figure 4-7 shows stresses for two cases: the elastic case with no fractures and the case giving the largest deformations (full fracture set, friction angle 20 degrees). Two sections are shown: One horizontal section 0.05 m below the tunnel floor, and one vertical section through the pillar between the central deposition hole and the neighbouring hole at x = 6 m. The plots show stress tensor symbols with colour codes regarding the major principal stress. The symbols are projections onto the viewing plane. The horizontal and vertical sections are not to scale: the width of the annular region around the deposition hole is 0.4 m, while the pillar width is 4.4 m.

The following can be observed:

- In both cases the maximum stress is found in the intersection between tunnel and deposition hole. This is because high tangential stresses develop both around the tunnel and around the deposition hole. Note that the hoop stress locations do not accord with the orientation of the initial stress field. This is because the tunnel excavation twisted the stress field clockwise below the tunnel. All this is logical and consistent with previous results /1-2/.

- The presence of fractures changes the distribution of stresses and creates discontinuities in the stress field. For the resolution used here (13 MPa/colour) this effect is obvious only along fractures that undergo significant slip (cf Figure 4-5).

- The maximum stress is about 16% larger in the fracture model compared to the elastic model. This applies for the 20 degree friction angle model shown here. Corresponding results for the models with 30 and 40 degree friction angle were 5% and 3% respectively.

- No stresses exceeding 100 MPa are found. Stresses exceeding 60 MPa are found only within regions of less than 0.1 m^3 totally in the elastic model and in about twice that volume in the fracture model. Stresses exceeding 75 MPa are found in even smaller regions (couple of dm^3).

Figure 4-8 shows the same stress tensor symbols, but here the colour code regards the minor principal stress. Only stresses in zones in which the minor stress is tensile are shown. Note that different resolutions apply for the elastic model (2.5 MPa/colour) and the fractured model (7.5 MPa/colour). The following can be observed:

- Tensile stresses are found, in particular in the floor region around the deposition hole and, for the fractured model, in small regions around fracture intersections. The magnitudes are however small: a couple of MPa.

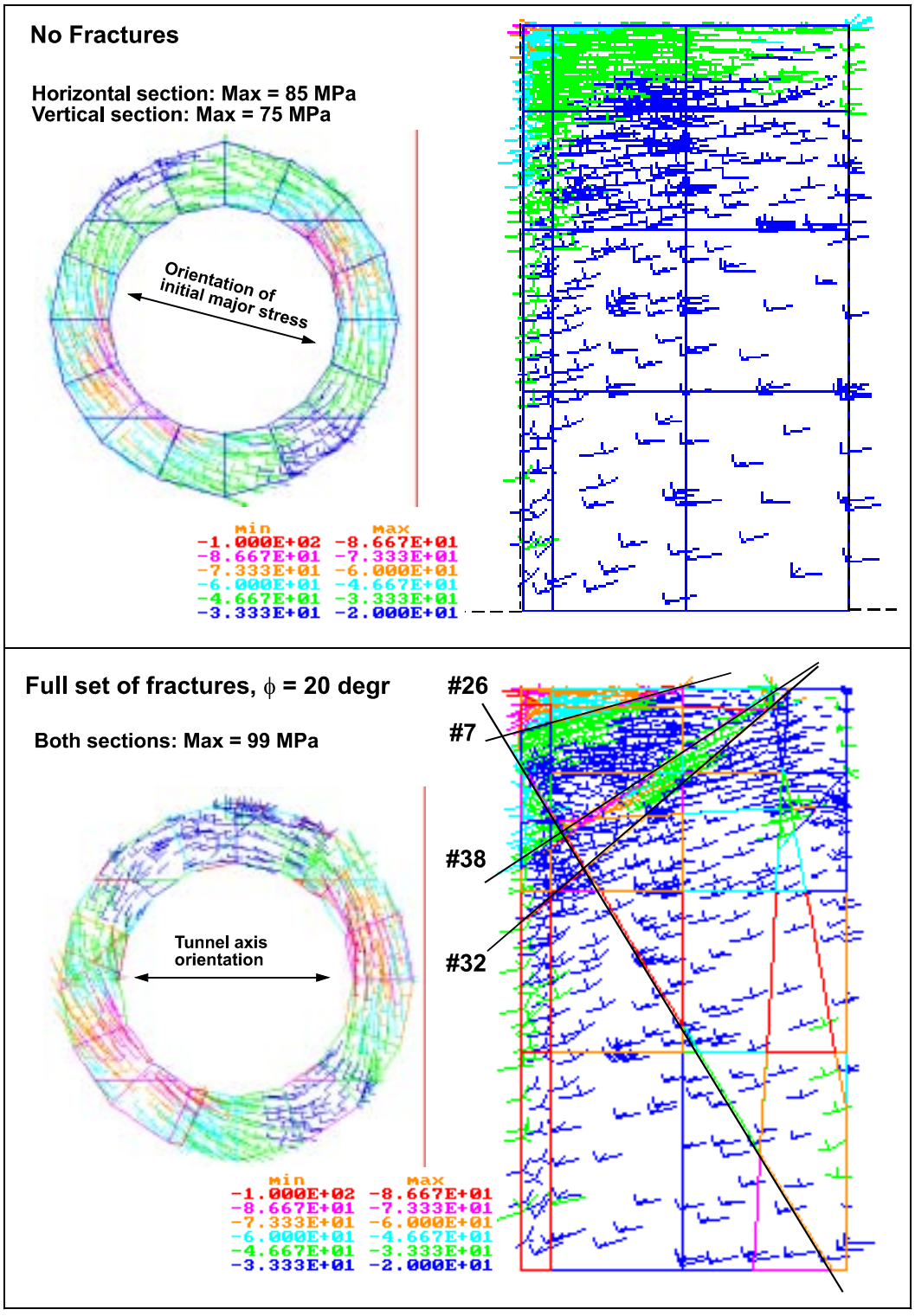

Figure 4-7. *Stresses in annular region around the central deposition hole and in the pillar between the central hole and the neighbour hole at x = 6 m. Colour code refers to major stress. Minus sign denotes compression.*

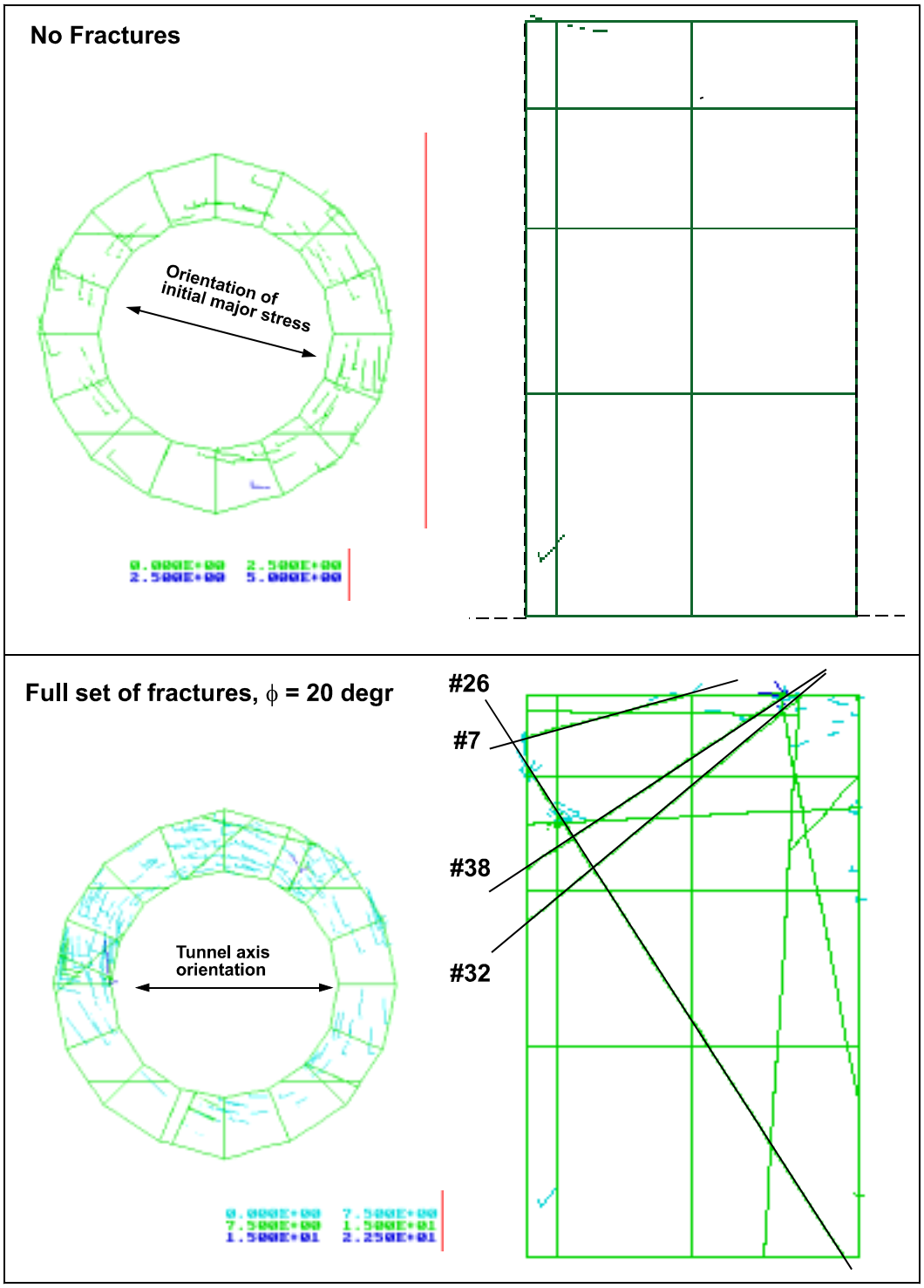

Figure 4-8. *Stresses in annular region around the central deposition hole and in the pillar between the central hole and the neighbour hole at x = 6 m. Colour code refers to minor stress. The plots show only tensile stresses.*

5 Supplementary analyses

5.1 General

The results presented in the preceding chapter show that the influence of the fracture system on the mechanical behaviour of the nearfield rock is modest, at least for the particular fracture geometry analysed here. The response to tunnel excavation and to deposition hole excavation was largely elastic in nature. It is not possible (with reasonable efforts) to analyse sufficiently many of the 30 FracMan realisations with 3DEC to be able to prove in a statistical sense that this is generally the case. However, some of the conditions (e.g. most fractures in high or reasonable compression, modest fracture frequency) that contribute towards stability will not vary between realisations. These conditions are general properties of the rock mass surrounding the TBM tunnel. Position and orientation of individual fractures relative to the excavated rooms will however vary. Cases may exist in which the interaction between one individual fracture and the tunnel, or between one individual fracture and the deposition hole, will cause instability. In this chapter, results from idealized analyses of simple generic models of such cases are presented.

5.2 Model description

The model dimensions are in principle identical to those of the model described in previous chapters. Five cases are considered as shown in Figure 5-1, each including one single fracture. The fractures have extensions of about 20 m, i.e. the same size as the largest fractures in the statistically derived model described in previous chapters.

The initial stress field is the same as in the statistically derived model, i.e. with principal stresses being 28.9 MPa, 15.2 MPa and 8.5 MPa. However, the principal stresses are aligned with the symmetry axes of the excavation geometry. Two stress states are considered: Stress state #1 (major principal stress horizontal and perpendicular to tunnel axis) and stress state #2 (major principal stress horizontal and perpendicular to tunnel axis). The left part of Figure 5-2 shows the initial stress states. Because of symmetry, only ¼ of the rock mass needs to be modelled. The right part of Figure 5-2 shows the inner part of the model.

The two symmetry planes have the function of mechanical mirrors. This means that in cases C, D and E the influence of two identical fractures are modelled.

As in the full model, fractures were modelled with a Mohr-Coulomb failure criterion without cohesion. Two cases of fracture shear strength were analysed: 30 degrees friction angle and zero friction.

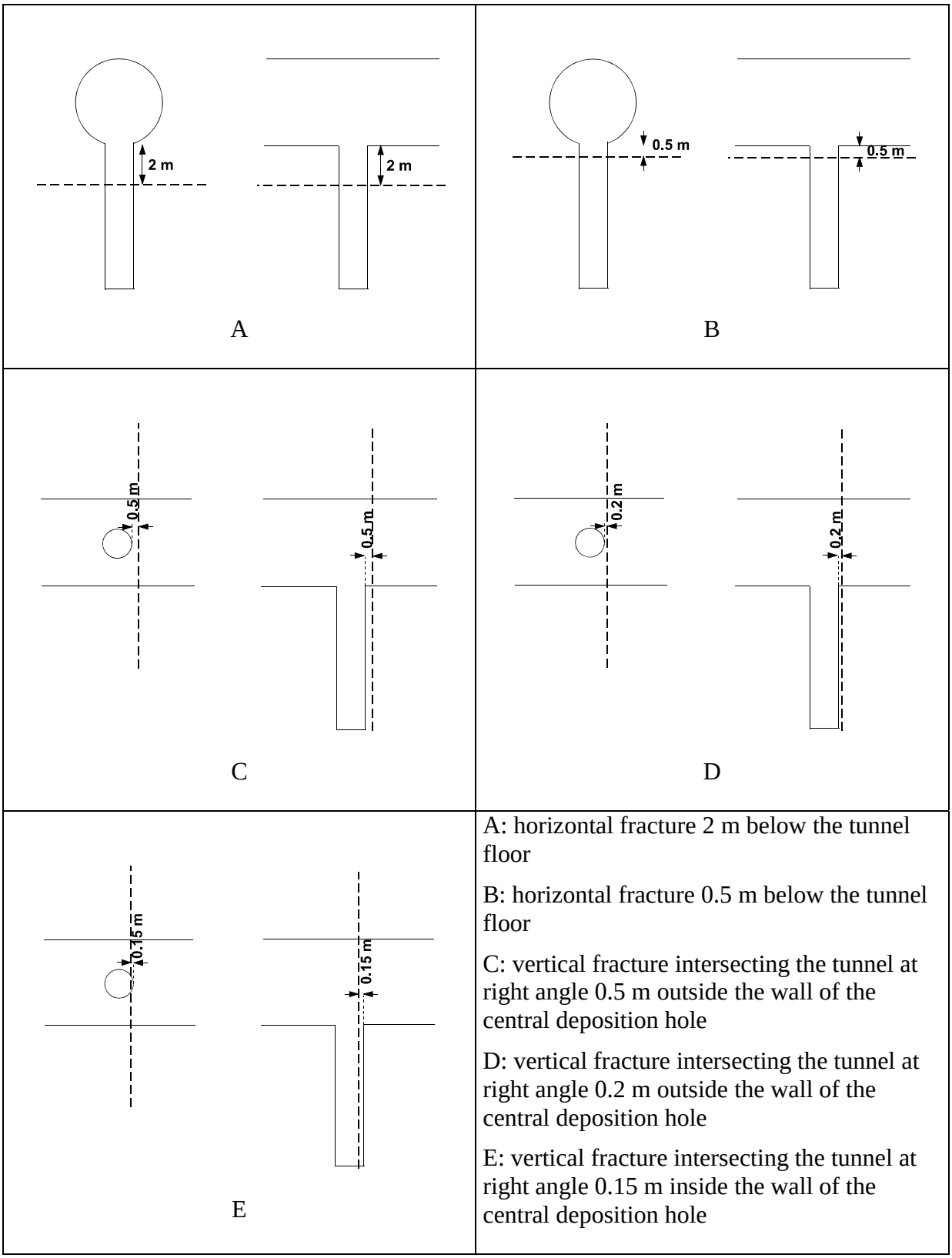

Figure 5-1*. Fracture geometries.*

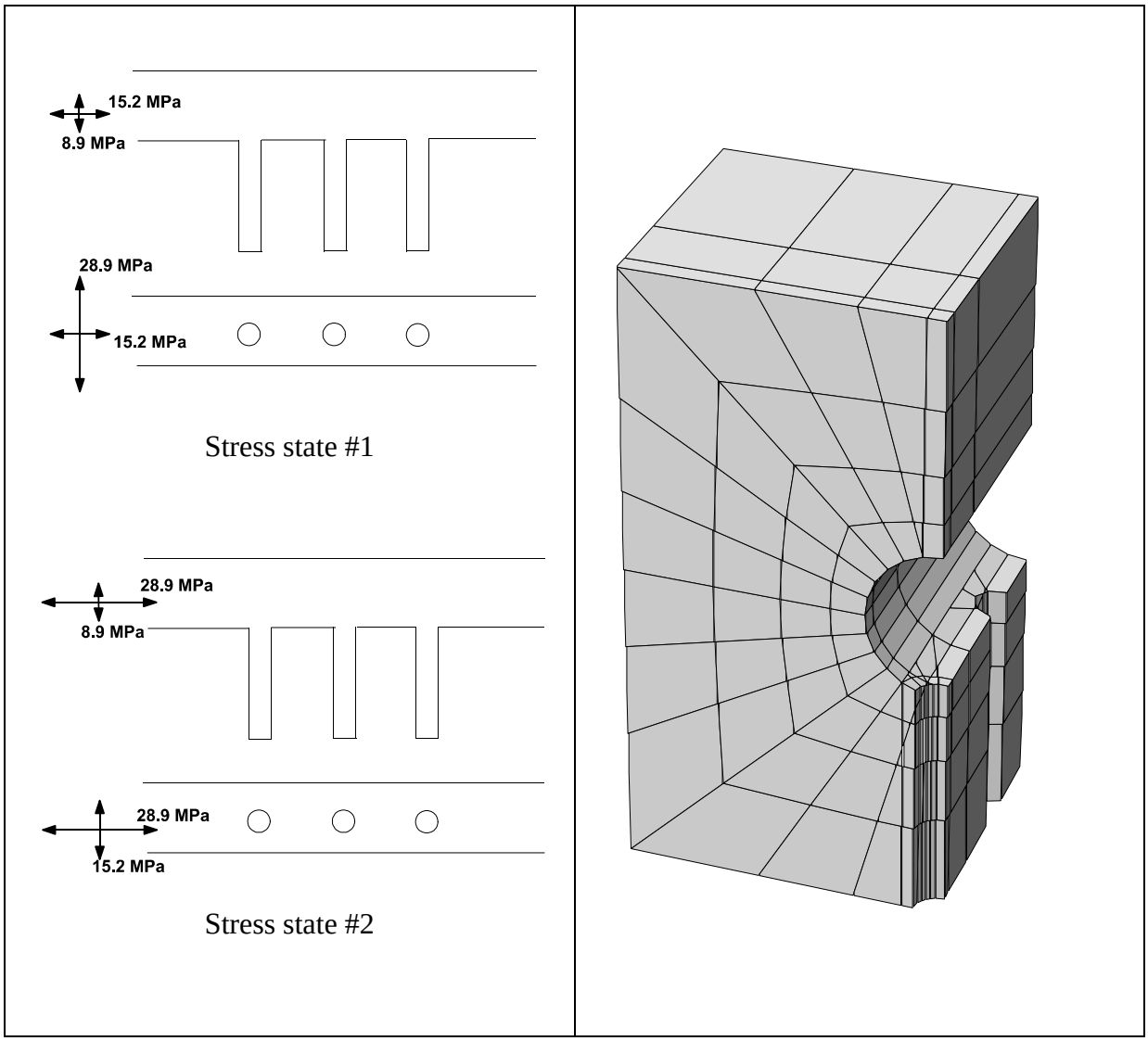

Figure 5-2. *Stress states (left) and inner part of the model (right). The case shown here is Case E (cf Figure 5-1)*

5.3 Results

5.3.1 General

In previous chapters it was shown that movements along fractures of the size that have been mapped in the TBM tunnel (about 15 m radius at maximum) did not change the excavation geometry much. This is consistent with analytical expressions that, for given loads and given elastic properties, give the maximum shear displacements as a function of fracture extension /5-1/. Figure 5-3 shows analytically calculated max shear displacements for a schematic and hypothetical load case, and points to the fundamental fact that it takes fractures of large extension to produce large shear displacements. Shear displacements of about 10 millimetres for instance, will require fractures that are several tens of meters in extension. In this section, the focus is on how stresses are affected by slipping fractures, i.e. by the presence of discontinuities that do not transfer shear stresses well, rather than on slip magnitudes.

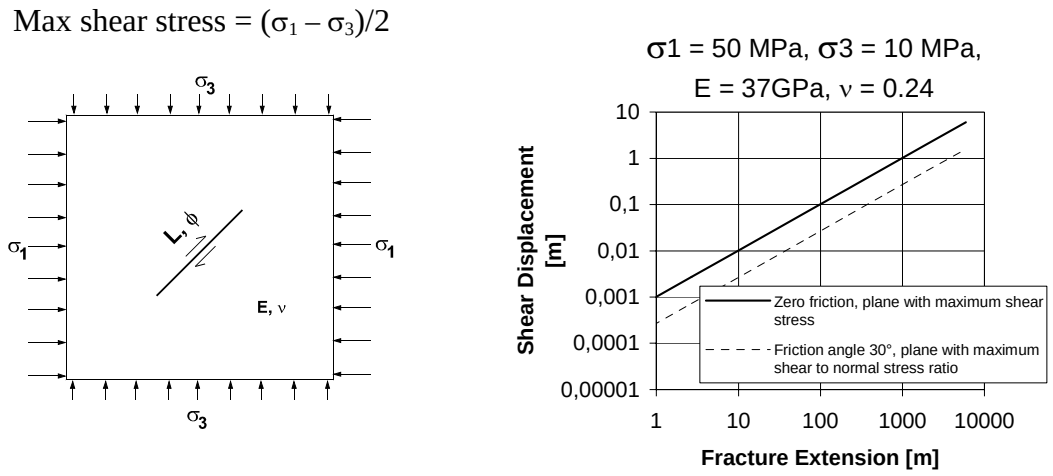

Figure 5-3*. Maximum shear displacement for fracture embedded in an elastic medium. From SR 97, processes in the repository evolution /5-2/.*

5.3.2 Rock displacements

Figure 5-4 shows displacements caused by excavation of tunnel and deposition hole. Only a few cases are shown. In both cases, the fracture is perpendicular to the tunnel. This means that the fracture did not have any significant influence during tunnel excavation, and that the slip effects seen in Figure 5-4 are due to the deposition hole excavation. The following observations can be made:

- If the fracture does not intersect the deposition hole, its influence on the general pattern of deformation is modest. In case D, the maximum deformation was about 34% larger than the maximum deformation obtained in the elastic case.

- If the fracture intersects the deposition hole such that the angle between the fracture and the periphery of the hole is oblique, then the displacement can be considerable (case E). In the next section (stresses) it is shown that the release of energy associated with these displacements results in significantly reduced tangential stresses.

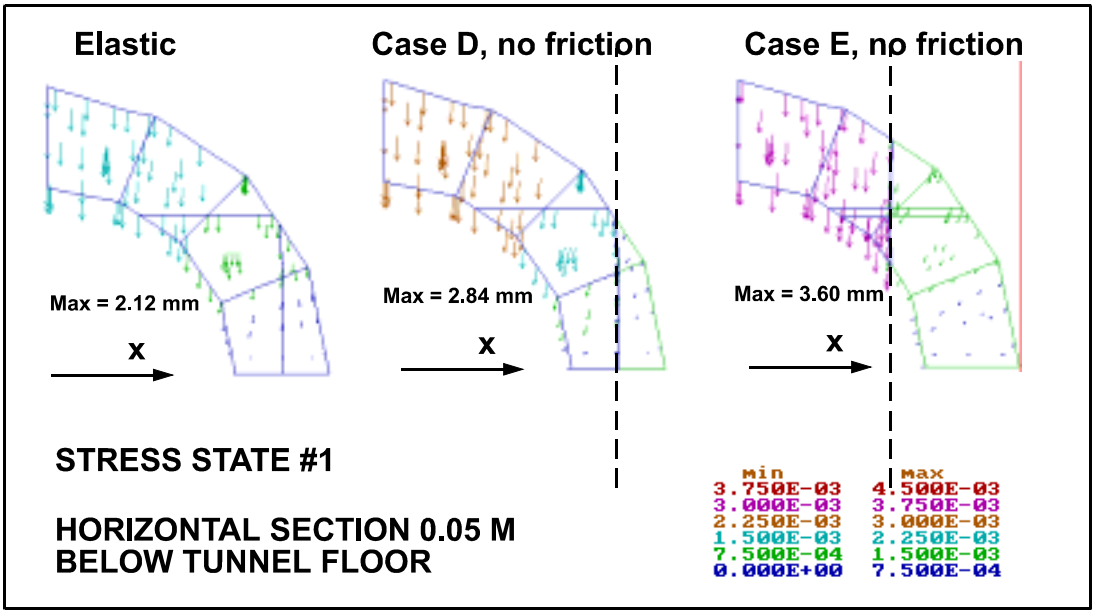

Figure 5-4. *Rock displacements in horizontal section through 0.4 m annular region around the deposition hole. The section is 0.05 m below the tunnel floor.*

5.3.3 Stresses

In all cases, the maximum stress is found where the deposition hole intersects the tunnel floor in point P (Figure 5-5).

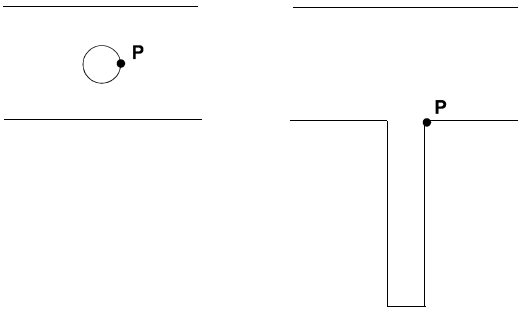

***Figure 5-5**. Point P where maximal stresses were found.*

Figures 5-6 and 5-7 show stresses in the upper part of the pillar between the central deposition hole and the neighbouring deposition hole at x = 6 m for a few selected cases. The contours of the deposition holes are outlined in the uppermost figures. An overview of the maximal stress (i.e. in point P) found in all models is given in Table 5-1.

The following can be observed:

- Stress state #1, major initial stress perpendicular to the tunnel, gives larger secondary stresses around the deposition hole than stress state #2. Without fractures the maximum stress amounts to about 155 MPa (Figure 5-6, Table 5-1) whereas corresponding value in the stress state #2 model is 65 MPa (Table 5-1). The region of high stress is however small: stresses in excess of 125 MPa are found only within 0.2 m from intersection point P.
- Fractures of large extension and low shear strength may change the stress state in the pillar (compared to the elastic stress distribution) in two fundamentally different ways. One way is general stress reduction as result of strain energy release caused by slip along fractures that intersect the excavation boundaries (Case E, cf Figure 5-3). One way is stress increase caused by localisation of force transfer to regions between the excavation boundaries and a nearby fracture (Cases A, B, C and D).
- If a stability estimate were based on the uniaxial compressive strength for the rock types in the Äspö HRL rock mass, then no intact rock failure would take place in any of the stress state #2 cases. (The uniaxial compressive strength of Äspö diorite, which makes up 91% of the TBM tunnel rock mass /5-3/ is 150 MPa at minimum with a mean of 183 MPa, as given by early measurements /5-4/. Measurements that are more recent have shown that the mean value is even higher: 219 MPa /5-5/).
- For stress state #1, failure could theoretically occur in all cases, including the elastic case.
- Regions of potential failure are small, even for cases that give very high stresses.

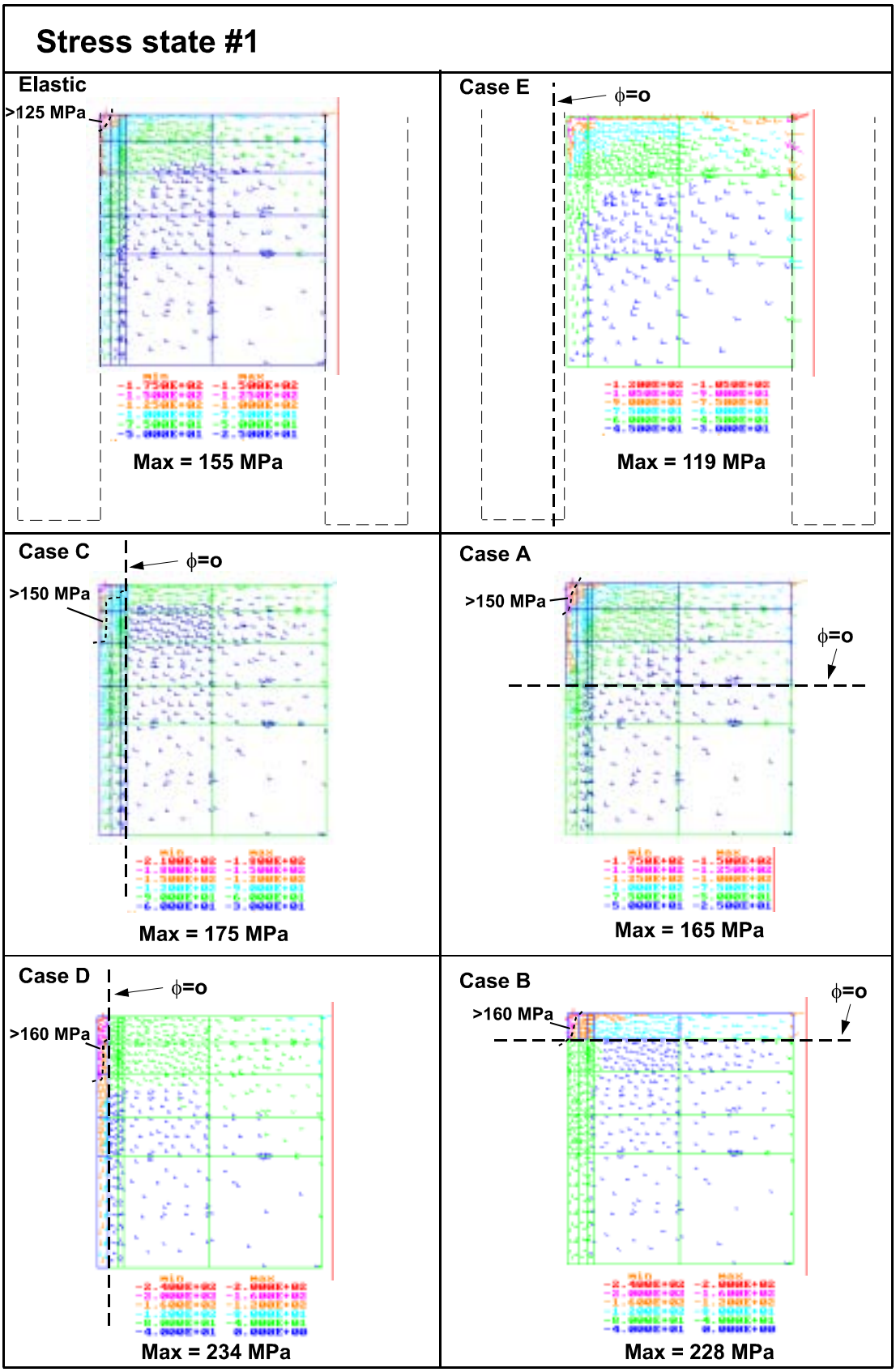

Figure 5-6. *Stresses in the upper part of the pillar.*

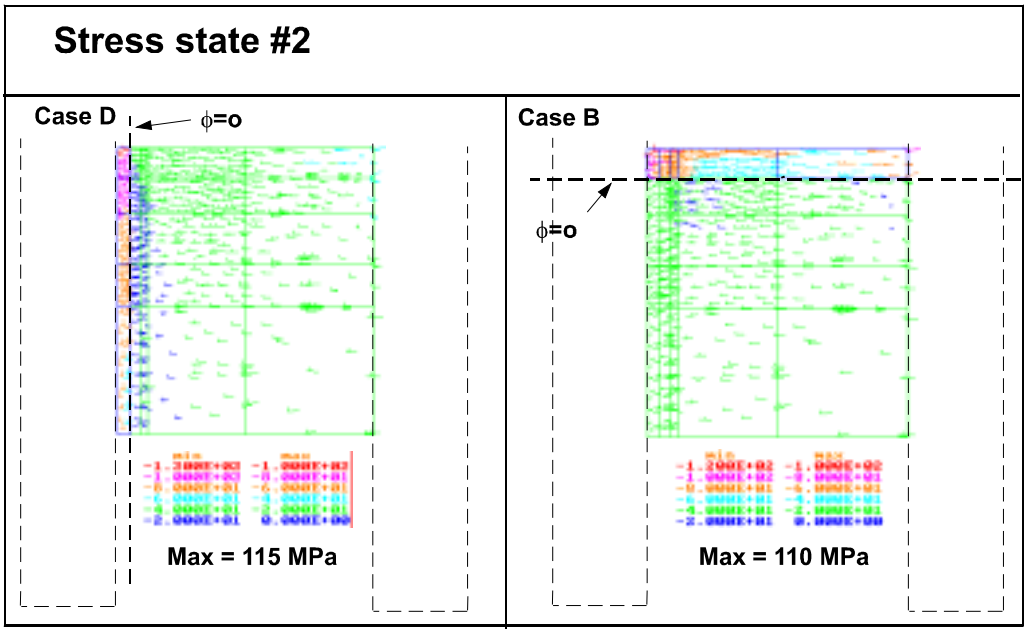

Figure 5-7. *Stresses in the upper part of the pillar.*

Table 5-1. Maximum stress (MPa) in intersection between tunnel and deposition hole.

		Stress state #1		Stress state #2	
Excavation		Tunnel	Hole	Tunnel	Hole
Elastic (no fractures)		80	155	40	65
Case A:	Horizontal fracture 2 m below floor				
	Friction 30 degr	81	158	41	67
	Friction 0 degr		165		72
Case B:	Horizontal fracture 0.5 m below floor				
	Friction 30 degr	97	189	48	67
	Friction 0 degr		228		110
Case C:	Vertical fracture 0.5 m from hole				
	Friction 30 degr	80	164	39	71
	Friction 0 degr		175		77
Case D:	Vertical fracture 0.2 m from hole				
	Friction 30 degr	80	194	39	93
	Friction 0 degr		234		115
Case E:	Vertical fracture 0.15 m inside hole				
	Friction 30 degr	80	120		
	Friction 0 degr		119		

6 Conclusions and discussion

6.1 Conclusions

The following general conclusions can be drawn:

- The types of fracture systems analysed here do not have a significant direct effect on the nearfield rock deformations that take place because of excavation of tunnel and deposition holes. The major part, between 70% and 95% depending on the assumptions made regarding fracture shear strength, of the deformations is due to immediate elastic response of the rock mass.

- In the region around tunnel/hole intersection, the mechanical response to excavation of tunnel and deposition hole is hardly influenced at all by fractures located at a couple of metres of distance from that region. Neglecting about 50% of the fractures within the 20 m cube did reduce the convergence of the deposition by not more than between 1% and 5%, depending on the assumptions made regarding the fracture shear strength.

- While the fractures do not have a decisive influence on the magnitudes of excavation-induced deformations, they may, because they do not transfer shear forces in their own plane well, single out regions of increased or decreased stresses. This may lead to intact rock failure in small regions and is probably the most important effect of the fractures when it comes to the mechanical stability of individual deposition holes.

- The effect of fracture displacements on stresses was modest in the calculations that were based on the TBM tunnel rock mass Discrete Fracture Network model. The results from the schematic models showed, however, that cases can be found for which slip along unfortunately located fractures, e.g. tangentially oriented fractures very close to the excavation boundaries, may give relatively high stresses.

- Regions where stresses increased sufficiently to produce immediate intact rock failure are found, in particular, between fractures and excavation boundaries. The most abundant rock type in the TBM tunnel rock mass is Äspö diorite (91%) /5-3/, with a measured uniaxial compressive strength ranging between 164 MPa and 217 MPa /5-4/. Assuming the uniaxial compressive strength to be 150 MPa, the following can be concluded:

  – No intact rock failures would be found in the full model (statistically generated fractures, initial major stress inclined 15 degrees with respect to the tunnel axis).

- No intact rock shear failures would be found in any of the cases where the initial major stress was parallel with the tunnel axis (stress state #2).

- If the initial major stress is perpendicular to the tunnel axis (stress state #1) then failure in the upper part of the deposition hole may occur even without the influence of fractures. Failure regions are however very small.

Recent measurements have given a mean compressive strength of 219 MPa and a minimum strength of 206 MPa for the Äspö Diorite /5-5/. If these values apply, immediate intact rock failure would occur only for the most conservative cases (stress state #1; nearby, low-strength fracture).

- The conclusion above applies also for delayed failures occurring at the crack damage level, i.e. at stresses corresponding to 80% of the laboratory determined uniaxial compressive strength, as suggested by Martin /6-1/. However, if even more conservative criteria are applied, for instance if it assumed that failure will occur in rock that has reached the crack initiation level (40% of the laboratory determined uniaxial compressive strength), then failures in small regions may theoretically occur even in some stress state #2 cases.

- The orientation of the initial stress field seems to be more important for creation of potential failure regions than the geometrical arrangement of fractures or the mechanical properties of the fractures.

6.2 Discussion

6.2.1 General

This report addresses the problem of mechanical stability of deposition holes.
The fracture system can have the following influences:

- Stress release along slipping fractures that intersect the periphery may influence the pattern of deformations such that the geometry of individual deposition holes degenerate.

- Wedge-shaped blocks may form because of rock removal and eventually separate from the walls.

- Tangential stresses may be so high that failure in the intact rock takes place, either immediately or some time after excavation. Such failures may also take place later when stresses increase further because of future loads.

From a mechanical viewpoint, these stability problems are important mainly during construction, i.e. before the emplacement of buffer and waste canister.

6.2.2 Change in deposition hole geometry

If the deposition hole geometry is disturbed because of extensive fracture slippage that takes place during the stand-up time after completion of the deposition hole, the necessary clearance between bentonite blocks and the walls of the deposition hole may be affected. This could theoretically obstruct the emplacement operation. The results obtained in this study show, however, that slipping fractures do not seem to affect the deposition hole geometry in any significant way. The initial clearance is about 50 mm, while slipping fracture effects are found to be about 1 mm for the most conservative cases. Consequently, this particular aspect of deposition hole stability does not appear to be of any concern during construction.

After emplacement, future loads may produce additional slippage and additional disturbances to the geometry but, to have any impact on long term safety, shear displacements must be 0.1 m or more /5-2/. This requires that the deposition hole intersects central parts of fractures with extension in their own plane of several 100 m /5-2/, /6-2/. Therefore, this aspect of deposition hole stability does not appear to be of any importance for long-term safety.

6.2.3 Wedge formation

The internal stresses of rock blocks, e.g. wedges, close to detaching themselves from the surrounding rock due to loss of mechanical interaction across block boundaries, are zero or very low. In the model analysed here, no such zero stress blocks were found. However, formation of wedge-shaped blocks is a stochastic problem, which means that many realisations of the statistical Discrete Fracture Network model need to be analysed in order to get an estimate of the probability of wedging in deposition holes. It is not realistic to perform that many mechanical analyses with 3DEC, but simpler approaches, based on geometry only, may be sufficient if forecasting the extent of wedging will be important.

6.2.4 Intact rock failure

The risk for intact rock failure, e.g. spalling, in tunnel walls and deposition hole walls is an issue that has been explicitly identified as a criterion when estimating the suitability of a potential repository site /6-3/. Spalling is a problem during construction and stand-up time but, as far as purely mechanical aspects are concerned, not for long term safety /5-2/. Indicators of risk for extensive spalling are high initial stresses and low compressive strength of the predominant rock types.

In this study, no plasticity model for the intact rock was used and, consequently, no assumptions regarding intact rock strength were made. The risk for failure could only be estimated by comparing the stresses around deposition holes and tunnels with hypothetical strength criteria. The general conclusion is that the orientation of the tunnels relative to the stress field is by far more important than the influence of the fracture system and that elastic analyses provide sufficiently accurate results, unless very specific assumptions are made regarding geometry and strength of nearby fractures.

6.2.5 Relevance of the model

The results regard mainly the region around the intersection between a deposition hole and a tunnel of circular cross section. In the floor region of horseshoe-shaped tunnels, the tangential stresses are smaller and possibly the regions of potential failure in the upper part of the deposition hole would look different. Johansson et al. analysed stresses around the upper part of deposition holes in horseshoe-shaped tunnels, and evaluated the stability by use of a brittle rock strength criterion /6-4/. The conclusions were similar to the ones drawn here: small regions of potential failure may be found in the floor intersection. No systematic comparison between results obtained for circular and horseshoe shaped tunnels has, however, been conducted. The most general conclusion, i.e. that a fracture system of the type assumed here is not decisive of the deposition hole stability, is however not likely to be dependent on the shape of the tunnel.

No account was taken of a possible EDZ around the periphery of the tunnel. The significance of this is not clear. Experimental experiences from URL in Canada indicate that the EDZ may be sufficiently stress-relaxed to prevent spalling in the uppermost parts of the deposition hole, even though the initial stresses are high enough to give spalling further down /6-5/. This may mean that neglecting EDZ effects is conservative.

The initial state of stress conforms reasonably well to general regression relations assumed to apply in Swedish bedrock. The initial stresses at Aberg (Äspö HRL) are more anisotropic with a higher major principal stress than at the other generic sites considered in the SR 97 safety analysis /6-6/. Thus, with respect to initial stresses, the model is probably realistic or conservative.

The fracture system assumed here is representative of the TBM tunnel rock mass with a fracture intensity of 0.47 m^2 of fracture area per cubic metre of rock mass. The statistical DFN model upon which the fracture geometry is based corresponds to data for the Aberg site. Corresponding DFN models for the Beberg and Ceberg sites have significantly lower fracture intensities /6-7/. Thus, with respect to fracture intensity, the model analysed here is probably realistic or conservative. The fact that not all fractures were included, i.e. that the fracture intensity was reduced below the DFN value in the outer parts of the model, did not seem to affect the results regarding stresses and deformations in the region around the central deposition hole. Thus, altogether, with respect to the influence of the fracture system on the results presented here, the geometrical representation of the fracture system is probably adequate.

References

1-1. **Itasca, 1993.** 3DEC, 3-D Distinct Element Code. Ver 1.5 Users Manual. Itasca consulting Group Inc, Minneapolis.

1-2. **Hökmark H, 1996.** Canister Positioning. Stage 1 Thermomechanical Nearfield rock Analysis, SKB Arbetsrapport D-96-014, Svensk Kärnbränslehantering AB.

3-1. **Follin S, Hermansson J, 1997.** A Discrete Fracture Network Model of the Äspö TBM Tunnel Rock Mass. SKB Arbetsrapport AR D-97-001. Svensk Kärnbränslehantering AB.

3-2. GEOTAB, Äspö sprickdatabas.

3-3. **Brady B, Brown E, 1993.** Rock Mechanics for underground mining. Chapman & Hall, London.

3-4. **Hökmark H, 1991.** Distinct element method modelling of fracture behaviour in near-field rock. Stripa Project Technical Report TR 91-01, Svensk Kärnbränslehantering AB.

3-5. **Barton N, Vik G, 1988.** Stage I joint characterisation and stage II preliminary prediction using small Core Samples. Stripa Project Report IR 88-08. Svensk Kärnbränslehantering AB.

3-6. **Olsson R, 1998.** Mechanical and Hydromechanical Behavior of Hard Rock Joints. PhD Thesis, Chalmers University of Technology, Göteborg.

3-7. **Litterbach N, Lee M, Struthers M, Stillborg B, 1994.** Virgin Stress Measurement Results, Boreholes KA2870A and KA3068A. SKB Progress Report 25-94-32, Svensk Kärnbränslehantering AB.

5-1. **Pollard D D, Segall P, 1987.** Theoretical displacements and stresses near fractures in rock: with application to faults, joints, veins, dikes and solution surfaces. Fracture Mechanics in Rock. Academic Press Inc Ltd, London.

5-2. **SKB, 1999.** SR 97 – Processes in the repository evolution. SKB TR 99-07, Svensk Kärnbränslehantering AB.

5-3. **Rhén I, Stanfors R, Wikberg P, Forsmark T, 1995.** Comparative study between the Cored Test Borehole KA3191F and the First 200 m Extension of the TBM Tunnel. SKB Progress Report PR 25-95-09, Svensk Kärnbränslehantering AB.

5-4. **Stille H, Olsson P, 1990.** Evaluation of Rock Mechanics. SKB Progress Report 25-90-08, Svensk Kärnbränslehantering AB.

5-5. **Nordlund E, Li C, Carlsson B, 1999.** Mechanical properties of the diorite in the prototype repository at Äspö HRL. Laboratory test. SKB Äspö HRL International Progress Report IPR-99-25, Svensk Kärnbränslehantering AB.

6-1. **Martin D, 1994.** TVO & SKB workshop on rock strength. SKB AR 94-59, Svensk Kärnbränslehantering AB.

6-2. **Hakami H, Olofsson S O, 2001.** Numerical modelling of fracture displacements due to thermal load from a KBS-3 type repository. SKB Technical Report, Svensk Kärnbränslehantering AB (in press).

6-3. **Andersson J, Ström A, Svemar C, Almén K-E, Ericsson L, 2000.** What requirements does the KBS-3 repository make on the host rock? Geoscientific suitability indicators and criteria for siting and site evaluation. SKB TR-00-12, Svensk Kärnbränslehantering AB.

6-4. **Johansson E, Hakala M, 1995.** Rock mechanical aspects of the critical depth for a KBS-3 type repository based on brittle rock criterion developed at URL in Canada. SKB AR D-95-014, Svensk Kärnbränslehantering AB.

6-5. F Mine-By Experiment Phase III – Heated Failure Tests. Technical Progress Report and Summary of Stage 3. AECL, Whiteshell Laboratories, Pinnawa, Manitoba.

6-6. **SKB, 1999.** SR 97 – Post closure safety. SKB TR-99-06, Svensk Kärnbränslehantering AB.

6-7. **LaPointe P, Cladohous T, Follin S, 1999.** Calculation of displacements on fractures intersecting canisters induced by earthquakes: Aberg, Beberg and Ceberg examples. SKB TR-99-03, Svensk Kärnbränslehantering AB.